Sensitivity of Satellite-Derived Tropospheric Temperature Trends to the Diurnal Cycle Adjustment

Carl A. Mears and Frank J. Wentz

Remote Sensing Systems, Santa Rosa, California

ABSTRACT

Temperature sounding microwave radiometers flown on polar-orbiting weather satellites provide a long-term, global-scale record of upper-atmosphere temperatures, beginning in late 1978 and continuing to the present. The focus of this paper is the midtropospheric measurements made by the Microwave Sounding Unit (MSU) channel 2 and the Advanced Microwave Sounding Unit (AMSU) channel 5. Previous versions of the Remote Sensing Systems (RSS) dataset have used a diurnal climatology derived from general circulation model output to remove the effects of drifting local measurement time. This paper presents evidence that this previous method is not sufficiently accurate and presents several alternative methods to optimize these adjustments using information from the satellite measurements themselves. These are used to construct a number of candidate climate data records using measurements from 15 MSU and AMSU satellites. The new methods result in improved agreement between measurements made by different satellites at the same time. A method is chosen based on an optimized second harmonic adjustment to produce a new version of the RSS dataset, version 4.0. The new dataset shows substantially increased global-scale warming relative to the previous version of the dataset, particularly after 1998. The new dataset shows more warming than most other midtropospheric data records constructed from the same set of satellites. It is also shown that the new dataset is consistent with long-term changes in total column water vapor over the tropical oceans, lending support to its long-term accuracy.

1. Introduction

Temperature sounding microwave radiometers flown on polar-orbiting weather satellites provide a long-term, global-scale record of upper-atmosphere temperatures. The record begins with the launch of the first Microwave Sounding Unit (MSU) on TIROS-N in late 1978. A series of eight additional MSU instruments provided a continuous record to 2005. A follow-on series of instruments, the Advanced Microwave Sounding Units (AMSU), began operation in mid-1998. The MSU instruments made sounding measurements using four channels. Thermal emission from atmospheric oxygen constitutes the major component of the measured radiance, with the maximum in the vertical weighting profile varying from near the surface in channel 1 to the lower stratosphere in channel 4. Channels 2, 3, and 4, which measure thick layers of the atmosphere centered in the midtroposphere, near the tropopause, and in the lower stratosphere, are relatively free of complicating effects of surface emission, clouds, and water vapor. AMSU channels 5, 7, and 9 correspond to the MSU channels 2, 3, and 4. Although both the MSU and AMSU data suffer from a number of calibration issues and time-varying biases, several groups, including our own, have merged the data from these instruments together into a single climate quality data record.

The focus of this paper is the midtropospheric measurements made by MSU channel 2 (MSU2) and AMSU channel 5 (AMSU5). We currently produce a gridded monthly dataset from these measurements by intercalibrating and merging together data from the nine MSU instruments and four of the AMSU instruments. The current version of this dataset, Remote Sensing Systems (RSS) version 3.3 (V3.3) has been available and continuously updated since 2009 (Mears and Wentz 2009).

The derivation of long-term trends in tropospheric temperature from satellite observations requires that the diurnally varying component for the observation be removed. This is because the local observation time for most of the satellites drifts over time (Christy et al. 2000; Mears and Wentz 2005), causing diurnal variations to be aliased into the long-term record. Ideally, we would like to use a highly accurate, independent source of atmospheric and surface temperature specify the diurnal cycle. Unfortunately, no such data are available. In RSS V3.3, we use the output of a general circulation model to construct a diurnal cycle climatology (Mears and Wentz 2009) and have studied the use of other models for this purpose (Mears et al. 2011). A similar approach, using a scaled version of the RSS diurnal cycle climatology, is used by NOAA's Satellite Applications and Research (STAR), version 3.0 (Zou et al. 2009) to produce their version of the MSU/AMSU dataset. The group at the University of Alabama, Huntville, uses a method based on the analysis of cross-scan differences to deduce the local diurnal slope (Christy et al. 2003). We show here that none of the models completely removes the effects of the diurnal cycle, confirming the earlier work by Po-Chedley et al. (Po-Chedley et al. 2015). An improved means of specifying the diurnal cycle is thus required to replace that solely derived from a global climate model. Po-Chedley et al. (2015) developed a harmonic method for removing biases related to satellite diurnal drift for temperature sounding instrument based on analysis of the satellite observations themselves. Observationally based methods have been used to derive the first two harmonics of the diurnal cycle for the High-Resolution Infrared Radiation Sounder (HIRS; Lindfors et al. 2011) and for the AMSU-B humidity sounder (Kottayil et al. 2013).

In this manuscript, we explore three alternative approaches to removing the effects of the diurnal cycle from AMSU-derived measurements.

1) Excluding parts of each satellites record during times of rapid drift in local observation time, which we call the ''minimal drift'' or MIN_DRIFT approach.

2) Use of two satellites (*Aqua* and *MetOp-A*) that did not drift in local measurement times as reference satellites to adjust the drifting satellites, which we call the ''reference satellite'' or REF_SAT approach.

3) Adjustment of GCM-derived diurnal cycles using information derived by comparing satellite observations at different local times, which we call the ''optimized'' or DIUR_OPT approach.

These three approaches yield similar results for AMSU measurements, giving us confidence to apply the DIUR_OPT approach to MSU-based derived measurements. We are forced to use the DIUR_OPT approach for MSU

TABLE 1. Satellites used in this study.

Satellite	Instrument type	Period considered in this study	Period used in V4.0 product
TIROS-N	MSU	12/1978–12/1979	12/1978–12/1979
NOAA-06	MSU	07/1979–03/1983	07/1979–03/1983
		12/1985–10/1986	12/1985–10/1986
NOAA-07	MSU	08/1981–02/1985	08/1981–02/1985
NOAA-08	MSU	06/1983–08/1985	06/1983–08/1985
NOAA-09	MSU	07/1985–02/1987	07/1985–02/1987
NOAA-10	MSU	12/1986–08/1991	12/1986–08/1991
NOAA-11	MSU	10/1988–12/1994	10/1988–12/1994
		08/1997–04/1998	08/1997–04/1998
NOAA-12	MSU	09/1991–11/1998	09/1991–11/1998
NOAA-14	MSU	07/1995–12/2004	07/1995–12/2004
NOAA-15	AMSU	08/1998–12/2014	08/1998–12/2010
Aqua	AMSU	08/2002–12/2012	08/2002–12/2009
NOAA-18	AMSU	07/2005–12/2014	07/2005–12/2014
MetOp-A	AMSU	06/2007–12/2014	06/2007–12/2014
NOAA-19	AMSU	04/2009–12/2014	04/2009–12/2014
MetOp-B	AMSU	02/2013–12/2014	02/2013–12/2014

because the historical pattern of measurement times for MSU precludes the use of the other methods.

To construct a new version of the RSS dataset, we choose the DIUR_OPT approach for both AMSU and MSU, using CCM3-derived diurnal cycle climatology as a starting point. The improvement of the diurnal adjustments represents a major upgrade to the RSS V3.3 TMT (midtropospheric temperature) dataset, resulting in a new dataset that we call RSS V4.0 TMT.

2. Satellite data sources and early processing steps

The starting point of our analysis is a set of gridded monthly antenna temperature data files (L2C) for all MSU and AMSU instruments. These are obtained by processing the L1B data files that are freely available from NOAA's Comprehensive Large Array-Data Stewardship System (CLASS) for NOAA and EUMETSAT satellites, and similar files from NASA for AMSU on *Aqua*. Table 1 shows the instrument type and the time period used for each of the satellites used in our study. We do not consider data from *NOAA-16* because it contains a large bias drift (Zou and Wang 2011) or from *NOAA-17* because its period of operation is too short to be useful. A number of processing steps, including adjustments to the satellite position and observation time, removal of duplicate and clearly erroneous data, and conversion from instrument counts to microwave radiance, are applied to the data as they are assembled into the $2.5° \times 2.5°$ gridded monthly files (Mears and Wentz 2009). These procedures are nearly identical to those performed for V3.3 and thus they are not important for the transition from V3.3 to V4.0. For convenience, the resulting mean radiances are reported

in temperature units. These radiances differ subtly from what the satellite community typically refers to as brightness temperatures, since no antenna pattern corrections have been applied. Thus we avoid the use of the term ''brightness temperature'' in this paper.

We note one important difference between the V3.3 and V4.0 unadjusted radiance data. All MSU data used in V4.0 were obtained from the NOAA CLASS archive. This was not true for V3.3, which included MSU data files obtained informally from NOAA personnel. Since this new version uses data that are available to all users, it represents a step forward in traceability for the RSS TMT dataset.

3. Overview of the adjustments applied to the gridded data

A number of adjustments and procedures are applied to the gridded radiance maps before they are combined together to form a merged climate data record. In the sections below, we describe each adjustment in the order that they are applied. The flowchart shown in Fig. 1 summarizes these steps.

a. Earth incidence angle

Both the MSU and AMSU instruments are cross-track scanning instruments and make observations at a wide range of observation angles. Each measurement is adjusted so that it corresponds to the nadir view. This is performed using a climatology of monthly radiance obtained by using a radiative transfer model (RTM) to simulate the radiance as a function of Earth incidence angle (EIA) for each grid point and month of year. The input for the RTM is the output of the MERRA reanalysis over the 7-yr period from 1980 to 1986. The most important effect of this adjustment is to reduce noise in the final merged product. A typical monthly $2.5° \times 2.5°$ grid cell contains measurements from a variety of incidence angles and the exact mix of incidence angles varies from location to location and month to month. Without the incidence angle adjustment, these variations would result in additional noise when measurements from different fields of view are combined.

There is also a small effect due to the reduction of each satellite's height as its orbit decays over time, thereby increasing the EIA (Wentz and Schabel 1998). For some MSU satellites, there is a pronounced left/right asymmetry, which is removed by fitting near-constant instrument roll angle during the incidence angle adjustments (Mears and Wentz 2009). None of the incidence angle adjustments applied lead to changes on multiyear time scales that are large compared to
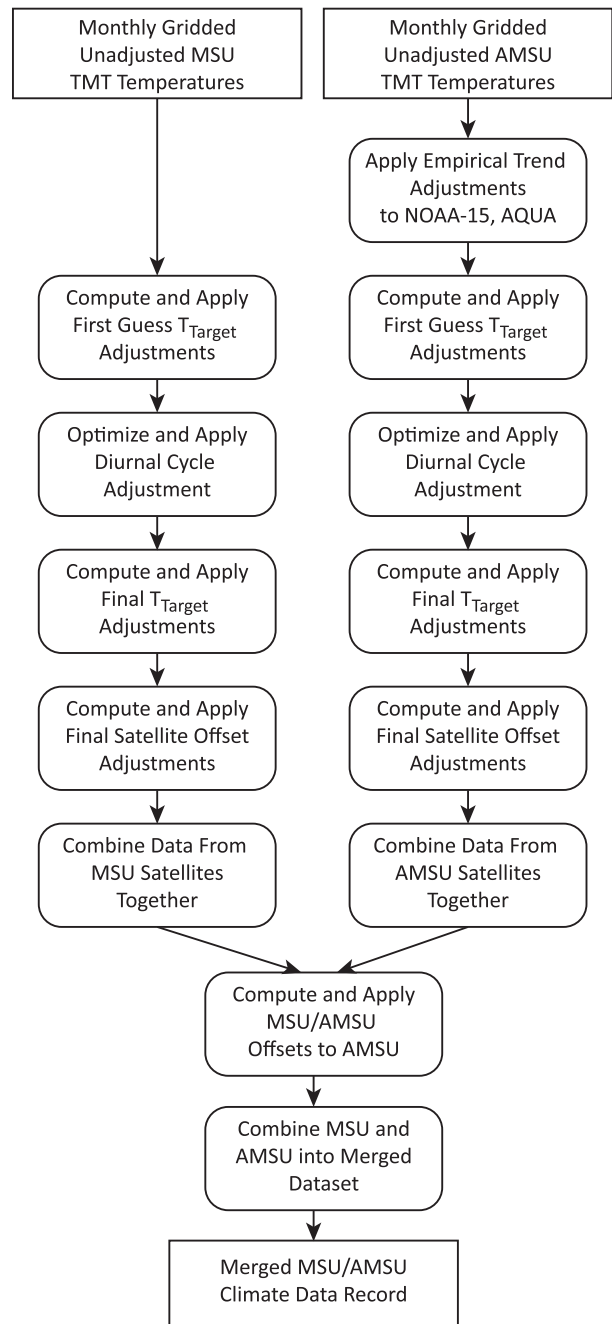

FIG. 1. Flowchart showing the adjustments applied to the MSU and AMSU gridded datasets prior to merging.

multiyear trends, but they do serve to slightly reduce spatial noise in gridded monthly means.

b. Diurnal cycle

Most of the satellites that fly an MSU or AMSU instrument have undergone substantial drifts in local measurement time (see Fig. 2). The exceptions are
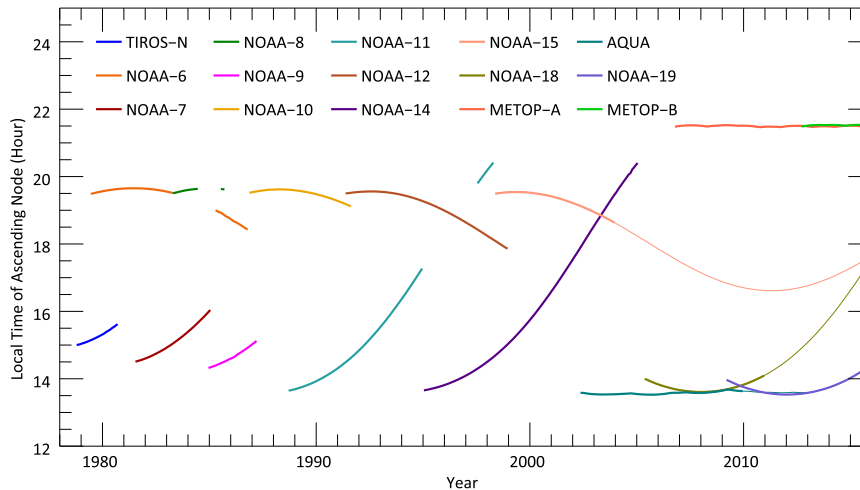
FIG. 2. Ascending local equator crossing time (LECT) for each of the satellites used. The LECT drifts over time for all satellites except *Aqua*, *MetOp-A*, and *MetOp-B*, which are maintained at constant local time by orbit keeping maneuvers. For the drifting AMSU satellites, the thinner lines denote the portion of the missions excluded in the MIN_DRIFT analysis.

NASA's *Aqua* satellite and the EUMETSAT *MetOp-A* and *MetOp-B* platforms, which use orbit-keeping maneuvers to maintain a nearly constant local measurement time. As the measurement times change for the drifting satellites, the changes in atmospheric and surface temperature due to the diurnal cycle are aliased into the long-term record. Thus it is necessary to characterize and remove the effects of changing measurement time.

For the previous versions of our dataset, our approach was to use a model-based diurnal climatology to adjust all measurements to correspond to a common local measurement time before performing subsequent merge steps. Version 3.3 used a gridded monthly average diurnal radiance climatology based on the Community Climate Model version 3 (CCM3) (Kiehl et al. 1996). The diurnal climatology was calculated by using the hourly output of the climate model as input to a radiative transfer model to find gridded, global-scale maps of the simulated radiance for each model time step. To obtain the diurnal climatology, the results for the same local time were averaged over the same month over 6 years (1979–84) of model output. In the current work, this adjustment is used as a starting point for the further diurnal adjustment optimization performed in section 3d, and derived in section 4.

c. Combine fields of view and ascending and descending nodes

At this point in the analysis, we combine the adjusted radiances from different fields of view into a single monthly map for each satellite and node (ascending or descending). For MSU, we use the central 9 (of 11 total) fields of view, and for AMSU we use the central 24 (of 30 total) fields of view. This is in contrast to what was done for V3.3 in which we used the central 5 fields of view for MSU, and the central 12 fields of view for AMSU. We find the inclusion of more fields of view results in reduced sampling noise in the monthly radiance maps. The inclusion of fields of view at larger Earth incidence angle makes it necessary to apply larger "limb corrections" (section 3a) to adjust the measurements so that they correspond to the nadir view. While these larger corrections may have larger random errors, these errors are likely to average toward zero when many corrected observations are averaged together. When we compare the long-term changes in V3.3 with a version of V4.0 with the same type of adjustments, the results are almost identical (see Fig. 8a). Finally, the ascending and descending nodes are also combined together, resulting in a single monthly map of radiances for each satellite. Combining the ascending and descending nodes is performed last to ensure that the ascending and descending nodes are equally weighted, so that the first harmonic of the diurnal cycle is accurately cancelled in nonpolar regions.

d. Additional diurnal adjustments

Because the diurnal adjustments made in section 3b are not perfect, we perform further adjustments for the REF_SAT and DIUR_OPT approaches. For the REF_SAT approach we adjust the data from each satellite so that it matches a reference dataset derived from non-drifting satellites. For the DIUR_OPT approach, we

add a small semidiurnal adjustment to the model-derived diurnal cycle. In both cases, the adjustments depend both on the latitude and on the surface type (land or ocean). The details of each adjustment will be discussed in much more detail in section 4.

e. Calibration target temperature

It has long been recognized that global averages of simultaneous measurements made by co-orbiting MSU and AMSU instruments differ by both a time-invariant intersatellite offset and an additional term that is strongly correlated with the variations in temperature of the hot calibration target (which is an integral component of the instrument and measurement technology) for each satellite (Christy et al. 2000). To describe these differences, we use an empirical error model for radiance incorporating the target temperature and scene temperature correlation (Mears and Wentz 2009),

$$T_{\text{MEAS},i} = T_0 + A_i + \alpha_i T_{\text{TARGET},i} + \varepsilon_i \qquad (1)$$

where $T_{\text{MEAS},i}$ is the radiance measured by the ith instrument (reported in temperature units), T_0 is the true radiance, A_i is the temperature offset for the ith instrument, α_i is a small multiplicative "target factor" describing the correlation of the measured antenna temperature with the temperature anomalies of the hot calibration target, $T_{\text{TARGET},I}$, and ε_i is an error term that contains additional uncorrelated, zero-mean errors due to instrumental noise and sampling effects. The merging parameters used for the V3.3 dataset were found using a regression procedure that minimized intersatellite differences between monthly averages. The same method is used here, although the exact results may differ because of the different adjustments applied before this step is performed (Mears et al. 2011).

f. Intersatellite offsets

Once the α_i values are determined, we then find the latitude-dependent offsets using a regression procedure for each 2.5° wide latitude band. In contrast to V3.3, where a single offset was found for each latitude, we now find latitude-dependent offsets for land and ocean surface types separately. In general, the offsets found for V4.0 are considerably smaller and vary much less with latitude than those found for V3.3 because a greater fraction of the intersatellite differences has been explained by the previous processing steps, and in particular by the improved diurnal adjustments.

g. Matching AMSU TMT to MSU TMT

The MSU and AMSU instruments measure with slightly different frequency bands, leading to differences in radiance that depend on the atmospheric profile and surface type. We use an empirical adjustment found by analyzing MSU–AMSU differences during the overlap period to adjust AMSU radiances so that they correspond to MSU radiances (Mears and Wentz 2009). The adjustment is a function of grid cell location and month of year but does not contain a long-term trend, so it cannot mask errors due to calibration or diurnal drifts.

4. Optimization of model-based diurnal adjustments

An accurate adjustment to remove the effects of changing measurement time is critical for the construction of a climate data record with useful long-term changes. In addition to the CCM3-based diurnal adjustment used in V3.3, we have also investigated the use of other diurnal climatologies and their effects on the final results. These additional climatologies were derived from the Hadley Center Global Environmental Model version 1 (HadGEM1; Johns et al. 2006; Martin et al. 2006) and NASA's Modern-Era Retrospective Analysis for Research and Applications (MERRA; Rienecker et al. 2011). Results using these different diurnal climatologies were used to estimate the uncertainty in the long-term trends (Mears et al. 2011). We found that for the tropospheric channels, the diurnal adjustment was the dominant source of uncertainty for interannual time scales, including decadal-scale trends.

To evaluate the accuracy of any applied diurnal adjustment we plot globally averaged monthly intersatellite differences for pairs of co-orbiting satellites separately for land and ocean scenes. These differences are calculated after the application of latitude-dependent intersatellite differences (section 3f) and differences that depend on the warm calibration target temperatures (section 3e) have been removed. Ideally, if all the adjustments applied were accurate, the satellite measurements should closely match each other, and these differences (and trends in these differences) should be very close to zero. We choose to plot land and ocean average separately because any errors in the diurnal adjustment are typically larger over land, leading to important differences between land and ocean scenes. This helps determine whether or not any differences found are due to diurnal cycle errors or to some other cause.

In Fig. 3, we show this type of plot for near-global (60°S–60°N) AMSU5 averages for a number of AMSU satellite pairs. For most of the pairs, the second satellite in the difference (the subtrahend) is chosen to be either *Aqua* or *MetOp-A*. These satellites were chosen because they are in controlled orbits with insignificant changes in local observations time. Thus any changes in the
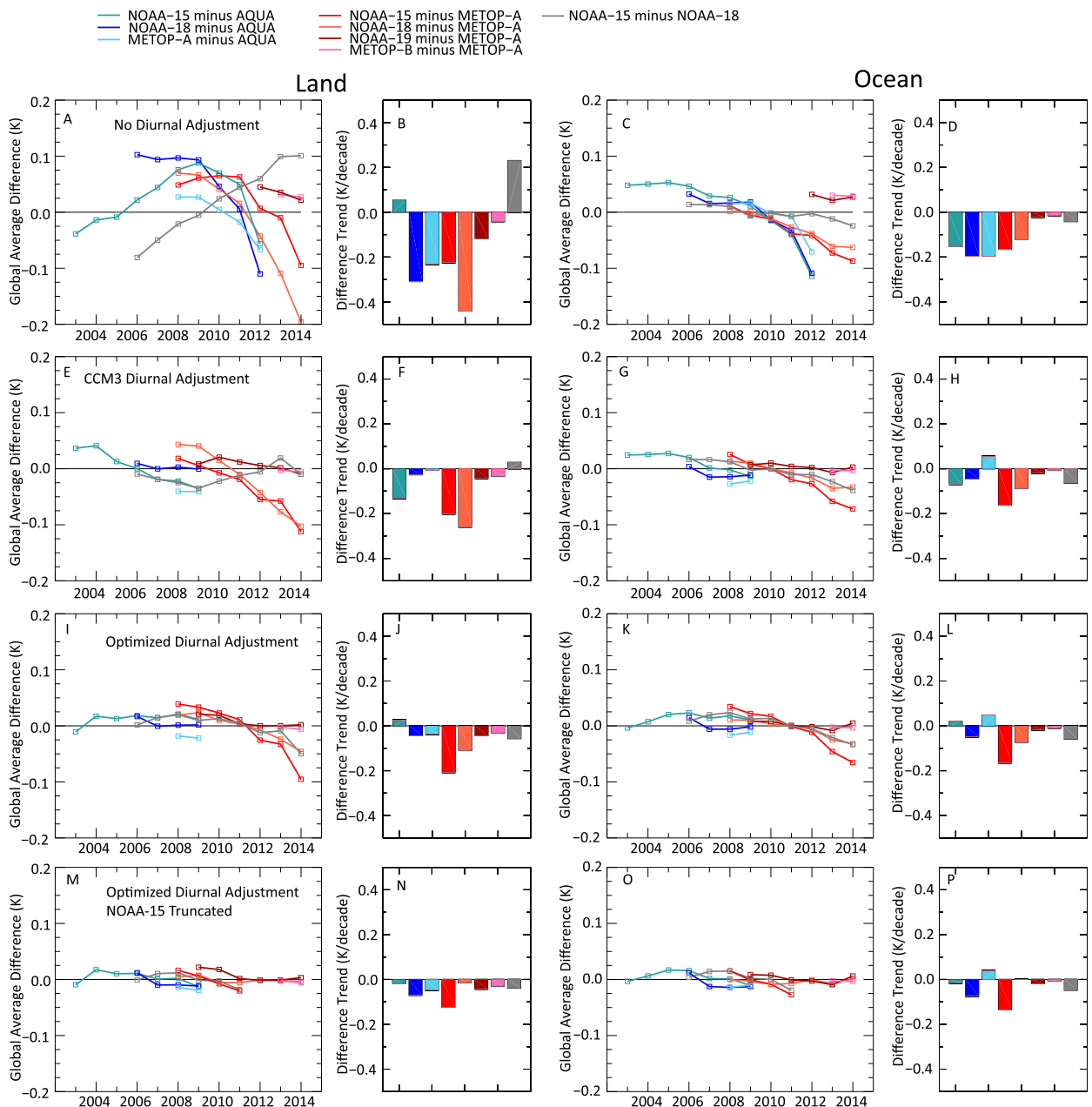
FIG. 3. Differences of yearly near-global (60°S–60°N) means between co-orbiting AMSU instruments with different levels of adjustment applied.

differences caused by the diurnal cycle are due to observing time changes for the first satellite. This makes it easier to evaluate whether or not the observed differences are consistent with changes in the measurement time.

The top row shows the results when no diurnal adjustment is applied. In this case, large intersatellite differences are present for both land and ocean scenes. We focus first on the ocean results, which depend less on the

diurnal adjustments. We note that the differences that involve *Aqua* all trend to large negative values starting in 2010. This corresponds to a period when increasing scan-to-scan noise suggests that this channel on *Aqua* is beginning to degrade (R. Spencer 2012, personal communication; also see Fig. S1 in the supplemental material, available online at http://dx.doi.org/10.1175/JCLI-D-15-0744.s1). Given the evidence for substantial instrument drift, we exclude *Aqua* data after December
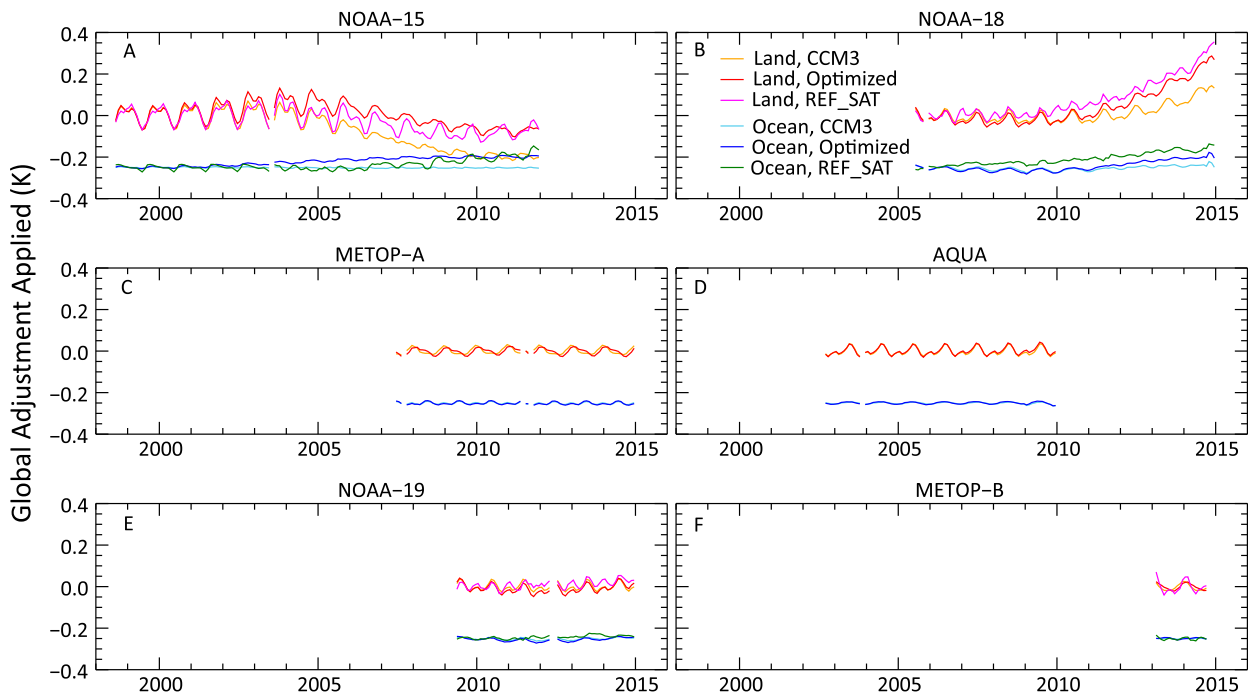
FIG. 4. Global-mean adjustments applied to each satellite using the original CCM3-based adjustments, and the optimized adjustment derived in this paper.

2009. We also note that the intersatellite differences for land are substantially larger for land than ocean. The most rapidly changing land differences tend to involve satellites (*NOAA-15* and *NOAA-18*) that drift rapidly in measurement time, indicating that the land differences are influenced by the diurnal cycle.

When we apply the CCM3-derived diurnal adjustments (second row in Fig. 3), the land trend differences are much reduced, showing that this adjustment is partially successful. The remaining differences, while more similar to the ocean differences, are still larger over land than over ocean (especially for *NOAA-18* minus *MetOp-A* after 2010, when *NOAA-18* drifts rapidly), indicating that the CCM3 diurnal adjustments are not perfect. Corresponding plots made using diurnal adjustments based on HadGEM1 and MERRA suggest that these diurnal adjustments contain errors that are at least as large over land, if not larger (see Fig. S2). A similar plot made for MSU2 indicates similar problems for the MSU2 diurnal correction. MSU2 will be discussed in section 4c (also see Fig. 6). The bottom two rows in Fig. 3 will be discussed in sections 4a and 4b below.

To visualize the effects of the CCM3 diurnal adjustments, Fig. 4 shows global averages of the original CCM3-modeled diurnal adjustments that we applied to each satellite. Given the evidence presented above that the CCM3 diurnal adjustment is an imperfect (but the

best of the model-based adjustments) improvement over the unadjusted data, we are motivated to try other approaches to reduce the effects of the errors in the CCM3 adjustment. For AMSU measurements, we investigate the three different approaches described below. For each of the approaches, we will investigate four different starting points. These are AMSU radiances with no model-based diurnal adjustments (NONE), and radiances adjusted by each of the three model-based adjustments (CCM3, HadGEM, and MERRA).

a. Using AMSU data with the minimum amount of diurnal drift (MIN_DRIFT)

The first approach we try is to construct a dataset that uses (to the extent possible) only those parts of the AMSU satellite record that do not have large changes in measurement time. This "minimal drift" analysis reduces (but does not eliminate) the sensitivity of the final results to measurement time drift and errors in the diurnal adjustment. The largest challenge to this approach is the *NOAA-15* and *Aqua* overlap. High-quality data from *Aqua* do not begin until September 2002. The *NOAA-15* measurement time has already begun to drift substantially by the end of 2001, and is close to its maximum drift rate by late 2002. At the same time, we desire a relatively long overlap with *Aqua* to be able to calculate accurate intersatellite offsets. We investigate the effects

TABLE 2. Global AMSU TMT trends (1999–2013; K decade^{-1}).

Diurnal model	Region	Model adjustment only	Model adjustment + MIN_DRIFT	Model adjustment + REF_SAT	Model adjustment + DIUR_OPT
None	Ocean	0.033	0.066	0.074	0.073
	Land	0.049	0.019	0.027	0.032
	Land + ocean	0.038	0.051	0.057	0.060
CCM3	Ocean	0.036	0.071	0.075	0.076
	Land	−0.016	0.047	0.046	0.061
	Land + ocean	0.015	0.063	0.065	0.071
HadGEM	Ocean	0.037	0.073	0.072	0.070
	Land	0.076	0.072	0.080	0.049
	Land + ocean	0.050	0.072	0.074	0.063
MERRA	Ocean	0.047	0.074	0.078	0.073
	Land	0.115	0.070	0.080	0.049
	Land + ocean	0.069	0.072	0.078	0.065

of using four different cutoff months for *NOAA-15* ranging from June 2003 to December 2004. We found that the global mean trend over the AMSU period was almost insensitive to the cutoff months, with changes ≤0.002 K decade^{-1}. We choose to perform further analysis using the December 2003 case, yielding 16 months of overlap time. We also choose to exclude *NOAA-18* after December 2011, excluding the period of rapid measurement time drift after this point. The excluded portions are shown by the thinner lines in Fig. 2. The 1999–2013, near-global AMSU-only trends that result from this analysis for each of the starting points are shown in Table 2. The use of the minimal drift dataset brings most of the global results from the different starting points into much better agreement than the case where all satellite months are used. The exception are the land-only results from the NONE case, where the minimum drift approach decreases the trend, increasing its difference from the others.

b. *Using* Aqua *and* MetOp-A *as a drift-free reference (REF_SAT)*

Our second approach is to use measurements from two of the AMSU satellites (*Aqua* and *MetOp-A*) that did not undergo measurement time drifts as a reference to determine adjustments to the drifting satellites. While these two satellites do not drift in measurement time, they do make observations seven hours apart. This difference, coupled with the seasonal modulation of the diurnal cycle, leads to a seasonally varying difference between the two satellites' measurements. We find it convenient to remove this difference and combine the measurements of the two satellites together to construct a single reference dataset. This is done by calculating a mean monthly *Aqua* minus *MetOp-A* difference for each 2.5° latitude band, separately for land and ocean, and then

using this difference to adjust *MetOp-A* so that the mean *MetOp-A* observations for each month of the year match the mean *Aqua* observations for that month. The *MetOp-A* and *Aqua* measurements are then combined to yield a combined reference dataset extending from September 2002 to December 2014.

The difference between each of the other satellites and this reference dataset is then calculated and used to adjust these satellites to correspond to the reference dataset. This will have the effect of removing both drifts due to changing measurement time and any other drifts that may be present, as well as eliminating the contribution of information from the adjusted satellites to the long-term changes. The measurements from the adjusted satellite will still serve to reduce sampling noise for individual grid points. The adjustment is performed by calculating the monthly zonal mean differences as a function of latitude for each satellite, separately for land and ocean scenes. These are then smoothed in both the north–south direction and in the time direction using a mean-of-three "boxcar" smooth. A disadvantage of this approach is that the drift-free reference does not begin until the start of the *Aqua* data in September 2002, and thus no differences for *NOAA-15* can be calculated before this time. We fill in the differences for this earlier time period by repeating the smoothed differences from September 2002 to August 2003 backward in time to extend the differences over the *NOAA-15* mission. This will clearly lead to some level of error, since the *NOAA-15* measurement time does drift during this earlier period, but the approach is likely to an improvement over performing no adjustments, especially for the cases where much of the diurnal cycle effects has already been removed by the model-based method.

Figure 4 shows global averages of the original CCM3-modeled diurnal adjustments and diurnal adjustments derived using the reference satellite method (using CCM3

as a starting point) for each satellite. (Figure 4 also shows the adjustments found by optimizing the model diurnal cycles, which is discussed in the next section.) The reference-derived adjustments are smaller for *NOAA-15*, and larger for *NOAA-18* than the model-derived adjustments. The 1999–2013, near-global, AMSU-only trends that result from this analysis for each of the starting points are shown in Table 2. The results are qualitatively similar to the "minimal drift" case. The results are closer together than the model-adjustment-only case, and agree with the minimal-drift case to within $0.01 \, \text{K decade}^{-1}$ for all starting points.

c. Optimizing the applied diurnal cycle (DIUR_OPT)

The third approach is to optimize the model-based diurnal cycles so that they more effectively remove the intersatellite differences. The diurnal adjustments are most sensitive to the second harmonic of the diurnal cycle. This is because (except for regions near the poles) the measurement times for the ascending and descending measurements are separated by approximately 12 h, so that the contributions from the odd harmonics cancel, and only the even harmonics $T_{\text{diurnal}}(t)$ are important for changes in the combined (ascending and descending) monthly means. This motivates us to introduce a second harmonic adjustment to T_{adj} to obtain T_{opt}, the optimized adjusted radiances:

$$T_{\text{opt}} = T_{\text{adj}} + a \sin(2\pi t_{\text{asc}}/12) + b \cos(2\pi t_{\text{asc}}/12) + c_i. \quad (2)$$

Here t_{asc} is the local time of the satellites ascending equator crossing; a and b are latitude and time-of-year dependent amplitudes and c_i is a satellite and scene-type dependent constant. We perform the adjustment separately for land and ocean scenes, since the land diurnal cycles are typically much larger than those for the ocean. Explicitly including the seasonal dependence of a and b we obtain the following:

$$\begin{aligned} T_{\text{opt}} = T_{\text{adj}} + c_i &+ [a_0 + a_1 \sin(2\pi m/12) + a_2 \cos(2\pi m/12)] \\ &\times \sin(2\pi t_{\text{asc}}/12) + [b_0 + b_1 \sin(2\pi m/12) \\ &+ b_2 \cos(2\pi m/12)] \cos(2\pi t_{\text{asc}}/12). \end{aligned} \quad (3)$$

Here m is the month of the year. We wish to choose values of the parameters (a, b, and c) that minimize the differences between observations made at the same time by different satellites. To do this, we form a system of equations from the monthly average intersatellite differences using all possible satellite pair–observation month combinations. For the ith and jth satellites, the equations in the system are of the following form:

$$\begin{aligned} T_{\text{opt},i} - T_{\text{opt},j} = T_{\text{adj},i} - T_{\text{adj},j} &+ a_0[\sin(2\pi t_i/12) - \sin(2\pi t_j/12)] + a_1 \sin(2\pi m/12)[\sin(2\pi t_i/12) - \sin(2\pi t_j/12)] \\ &+ a_2 \cos(2\pi m/12)[\sin(2\pi t_i/12) - \sin(2\pi t_j/12)] + b_0[\cos(2\pi t_i/12) - \cos(2\pi t_j/12)] \\ &+ b_1 \sin(2\pi m/12)[\cos(2\pi t_i/12) - \cos(2\pi t_j/12)] + b_2 \cos(2\pi m/12)[\cos(2\pi t_i/12) \\ &- \cos(2\pi t_j/12)] + c_n - c_m. \end{aligned} \quad (4)$$

Here, t_i and t_j are the ascending equator crossing times of each satellite. Note that the parameters a and b are the same for all satellites. The system is linear in the parameters (a, b, and c values) and the differences $T_{\text{opt},i} - T_{\text{opt},j}$ can be minimized using singular value decomposition to obtain optimal values of a and b for each latitude and surface type. In practice, we found it useful to calculate these values using mean values of T_{adj} averaged over a 12.5° wide latitude band, and then assign the solution to the 2.5° latitude band at the center of the wider band. This serves to provide smoothed a and b values as a function of latitude and reduce the effects of sampling noise. The constants c_n and c_m are not stored because they will be recalculated and removed when the intersatellite offsets are computed (section 3f). The amplitude and phase associated with a_0 and b_0 (the

annual mean values) for AMSU5 are plotted as a function of latitude in Fig. S3. The fitted values for seasonal modulation parameters ($a_1, a_2, b_1,$ and b_2) are much smaller than the annual mean amplitude except near the South Pole. The values of a_0 and b_0 are almost always smaller for ocean scenes than for land scenes as expected since the larger land diurnal cycles are likely to have larger errors.

Using the land and ocean values for the a and b terms, we calculate an optimized version of the model-based diurnal cycle climatology. The diurnal cycle for each grid cell is modified by adding the appropriate (land or ocean) second harmonic components. The modifications to grid cells that are partly land and ocean are adjusted using a weighted average of the land and ocean adjustments. We then use the optimized diurnal cycle to adjust the AMSU radiances to correspond to local midnight.
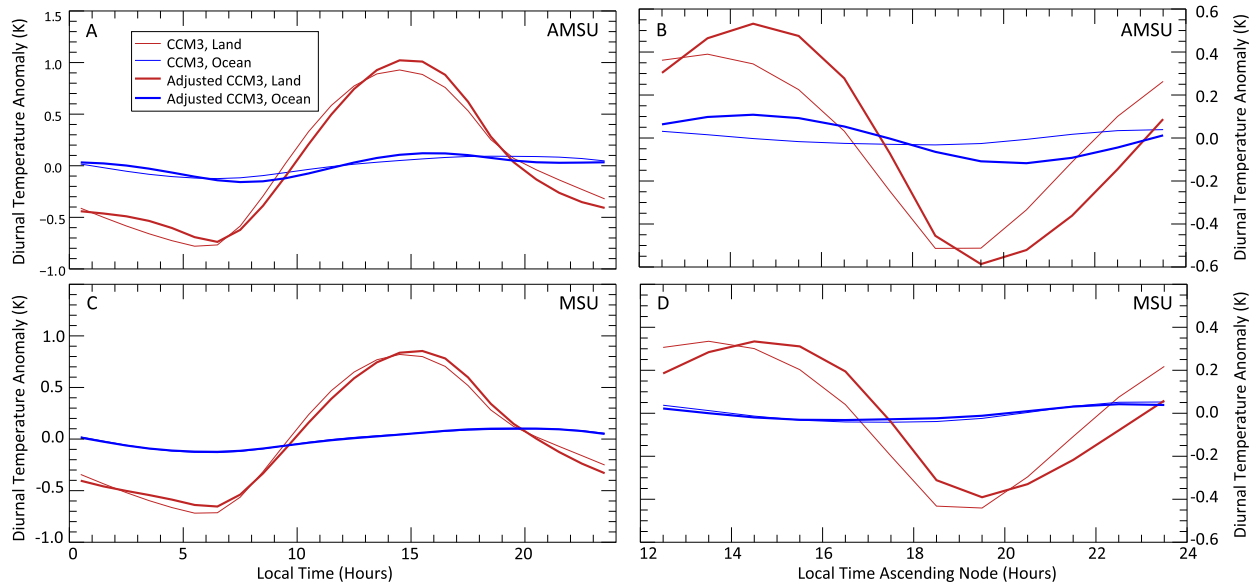
FIG. 5. (a),(c) Near-global mean (60°S–60°N) diurnal cycles from CCM3 for AMSU and MSU, before and after optimization using satellite measurements. (b),(d) Combined morning and afternoon diurnal adjustments, before and after optimization.

The postadjustment intersatellite differences are computed and shown in the third row of Fig. 3. This row is analogous to the row above it, except that the new diurnal adjustments are used. After applying the optimized diurnal adjustments, the land differences are reduced relative to the nonoptimized diurnal adjustments, and are similar to the ocean differences.

Near the poles, we might expect this procedure would not work as well, because the time difference between ascending and descending measurements begins to substantially differ from 12 hours. This means that the first harmonic of the diurnal cycle begins to become important poleward of about 65°, violating our assumption that only a second harmonic adjustment is needed. To investigate this problem, we evaluated Hovmöller diagrams of intersatellite differences as a function of time and latitude for each satellite pair (an example is shown in Fig. S4). We found that our procedure successfully reduced long-term trends at all latitudes, despite its formal shortcomings. We speculate that this is because the maximum satellite drift is substantially less than 12 h, allowing slopes caused by first harmonic effects to be successfully modeled by second harmonic adjustments.

Evaluation of the results in the third row of Fig. 3 shows that the largest remaining differences are for differences that include NOAA-15 after 2011, leading us to suspect that late in its lifetime NOAA-15 underwent a substantial calibration drift. It is unlikely that the cause of the observed differences is a problem with the diurnal cycle. The drift in observation time in NOAA-15

reversed in early 2011, but there is no such reversal in the NOAA-15 minus NOAA-18 and NOAA-15 minus MetOp-A differences. The presence of this drift leads us to exclude NOAA-15 measurements after December 2011 from the diurnal optimization and merging procedures. The bottom row in Fig. 3 results after removal of the NOAA-15 measurements after December 2011. Most of the intersatellite differences are quite small for both land and ocean. Note that the difference between NOAA-18 and MetOp-A, which had substantial slope when the NOAA-15 data was not truncated, now has a slope very close to zero. We suspect that this is because the erroneous NOAA-15 data after December 2011 were affecting the diurnal cycle optimization, leading to an erroneous diurnal cycle. This in turn led to a spurious drift in the adjusted NOAA-18 radiances. With this effect removed, NOAA-18 now agrees with MetOp-A. The effect of this change on the global mean trend is fairly minor. If the post 2011 NOAA-15 data were included, the 1988–2014 AMSU trend would decrease by $0.004 \, \mathrm{K \, decade^{-1}}$. We note that if the Aqua data, which we excluded because of excess noise after December 2009, were also included the 1988–2013 AMSU trend would increase by $0.035 \, \mathrm{K \, decade^{-1}}$, more than canceling the effects of excluding the post-2011 NOAA-15 data.

Figure 4 shows global averages of the original CCM3-modeled diurnal adjustments and the optimized diurnal adjustments that we applied to each satellite. The effect of the optimization is to reduce the land adjustment applied to NOAA-15 and NOAA-18, while slightly increasing the ocean adjustments to these satellites. The
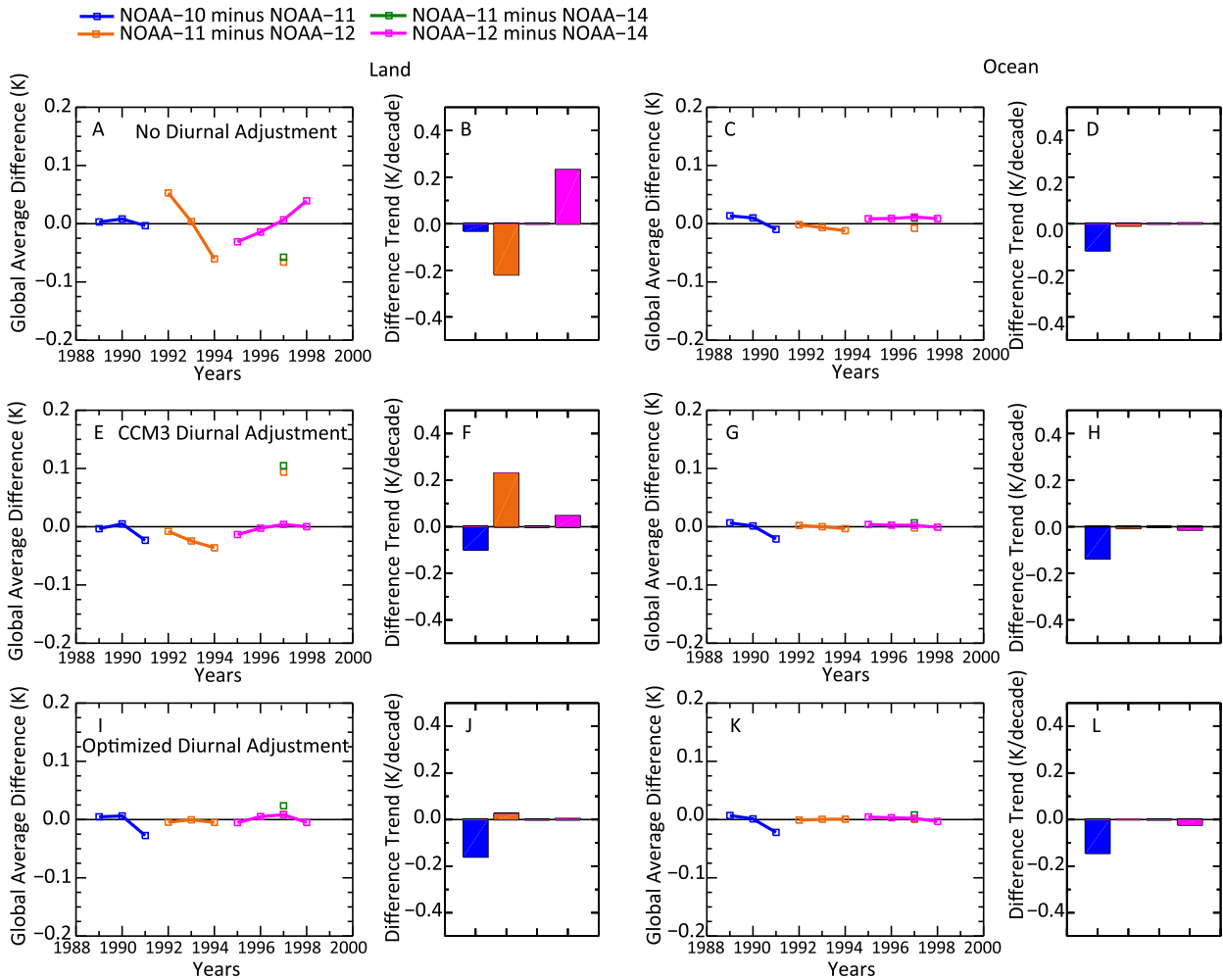
FIG. 6. Differences of yearly near global (60°S–60°N) means between selected co-orbiting MSU instruments with different sets of adjustments applied.

changes in adjustments to the other satellites are small, due to their small drifts in measurement time. Figure 5a shows near-global averages of the CCM3-derived diurnal cycle for AMSU before and after optimization. The main effect of the optimization is to delay the afternoon peak in the land diurnal cycle by about an hour, and increase the amplitude slightly. Figure 5b shows the morning and afternoon parts of the diurnal cycle combined so that only the even harmonics remain, causing the net effect on the adjusted radiance to be easily seen. Again, the peak of the land diurnal cycle is moved later in the day, and the ocean diurnal cycle adjustment is increased and now peaks at roughly the same time as the land diurnal cycle.

We repeated the above procedure using other diurnal adjustments as the starting point, including NONE (no adjustment applied), and the HadGEM1 and MERRA diurnal adjustments discussed above. In Table 2, we

summarize the near-global (60°S–60°N) trends in the merged AMSU data for the 1999–2013 period for both the optimized and nonoptimized diurnal cycles. Without the optimization of the diurnal adjustments, there is a large spread for the results from the different diurnal adjustments, particularly for land-only averages (−0.016 to 0.115 K decade^{-1}). After the optimization procedure, the spread in trends is reduced for both ocean and land averages.

d. Choosing an approach

The overall conclusion from the previous three sections is that the results of the three different approaches are in good agreement with each other. What remains is to choose a method to produce a final dataset. We choose to use the DIUR_OPT method because this is the only method that can also be used to improve the diurnal adjustment for MSU. For MSU, only the

"morning" satellites with equator crossing times in the 6:00 to 8:00 a.m. range show low drift rates. These do not have sufficient overlap to construct a MIN_DIUR subset of the data. All MSU satellites are in drifting orbits, making the REF_SAT method impossible. We choose to use a model-based diurnal cycle as the starting point to preserve the information from the model about differences in the diurnal cycle between different locations (e.g., desert vs. forest), and at different times of the year. While in principle it is possible to derive an optimized diurnal cycle at each grid cell, in practice the quality of the fits is compromised by sampling noise in the individual grid cell measurements. We then choose the CCM3 model because it appears to do the best job of the three models we have available of removing the effects of the diurnal cycle without adjustments.

e. Diurnal adjustment optimization for MSU

We now turn our attention to applying the DIUR_OPT method to MSU. The MSU analysis is challenging because the lengths of intersatellite overlaps tend to be much shorter, making it more difficult to obtain useful information from intersatellite comparisons. Although all data are used in the analysis described here, for plotting purposes we focus on the latter part of the MSU mission (satellites *NOAA-10*, *NOAA-11*, *NOAA-12*, *NOAA-14*) where longer satellite overlaps occur more often and thus the effects of our adjustments are easier to discern. Figure 6 is analogous to Fig. 3, except results from the four MSU satellites are plotted. The top row shows the yearly, near-global (60°S–60°N) intersatellite differences for land (left) and ocean (right) scenes with no diurnal adjustment. There are clearly large trends in the land differences, indicating that diurnal adjustments are necessary. The second row shows the results after the CCM3 diurnal adjustments are applied. The land trends are much reduced, but still clearly non zero, and the single points associated with *NOAA-11* minus *NOAA-12* and *NOAA-11* minus *NOAA-14* for 1997 (after *NOAA-11* again became operational for a brief period) have changed sign. We apply the same DIUR_OPT procedure to MSU (using all satellite overlaps as input, not just the ones shown here). This process results in adjustments to the CCM3 diurnal cycle similar in magnitude to those found for AMSU. Figures 5c and 5d show the unadjusted and optimized global mean diurnal cycle and diurnal adjustments for MSU. As was the case for AMSU, the afternoon peak is shifted slightly later, and the early morning slope is reduced for the land diurnal cycle. We do not expect that the MSU and AMSU diurnal cycles are the same, because AMSU makes measurements at a different frequency that allows more surface emission to contribute to the measured radiance.
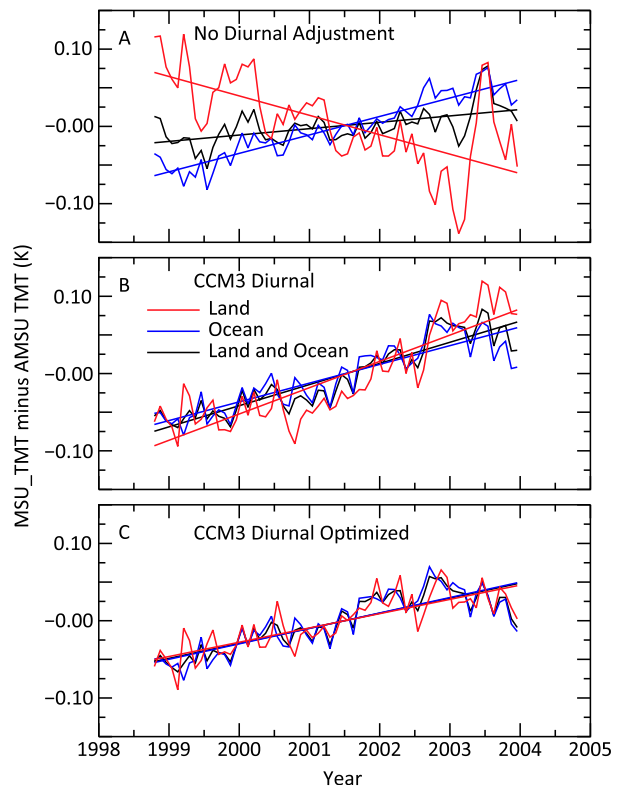

FIG. 7. MSU minus AMSU near-global (60°S–60°N) time series for land, ocean, and combined land and ocean regions. Each panel shows the results after different levels of adjustments are applied to the data.

When the MSU diurnal cycle adjustments are included in the CCM3 diurnal adjustment, the intersatellite slopes are substantially reduced (Fig. 6, bottom row), although the *NOAA-10* minus *NOAA-11* slope is still nonzero due to a relatively large difference in 1991 that appears for both land and ocean scenes.

f. MSU/AMSU difference trends

One of the unexplained mysteries of the previous version of our analysis (V3.3) was a large positive trend in the MSU minus AMSU differences during the period of overlap from late 1998 until mid-2002, followed by a period of smaller negative trend from mid-2002 until late 2003. The origin of these differences is not known. We included the effects of this difference trend into the uncertainty estimate for the V3.3 dataset (Mears et al. 2011). This mystery remains in the version of the dataset even after the optimization of the diurnal adjustments for MSU and AMSU. Figure 7 shows time series of merged MSU minus merged AMSU near-global (60°S–60°N) TMT differences over the period of overlap with varying levels of diurnal correction applied. Land-only, ocean-only, and land-and-ocean averages are plotted.

TABLE 3. Global MSU TMT trends (1979–2004; K decade^{-1}).

Diurnal model	Region	Model adjustments only	Model adjustments + DIUR_OPT
None	Ocean	0.097	0.125
	Land	0.052	0.175
	Land + ocean	0.082	0.142
CCM3	Ocean	0.103	0.120
	Land	0.108	0.190
	Land + ocean	0.106	0.143
HadGEM	Ocean	0.109	0.118
	Land	0.226	0.187
	Land + ocean	0.147	0.140
MERRA	Ocean	0.109	0.120
	Land	0.214	0.186
	Land + ocean	0.143	0.141

TABLE 4. Global MSU/AMSU TMT trends (1979–2014; K decade^{-1}).

Diurnal model	Region	Model adjustments	Diurnal optimized
None	Ocean	0.095	0.113
	Land	0.013	0.130
	Land + ocean	0.069	0.119
CCM3	Ocean	0.086	0.110
	Land	0.065	0.155
	Land + ocean	0.079	0.125
HadGEM	Ocean	0.092	0.109
	Land	0.195	0.151
	Land + ocean	0.125	0.122
MERRA	Ocean	0.093	0.109
	Land	0.193	0.148
	Land + ocean	0.125	0.121

Figure 7a shows the differences with no diurnal adjustments applied. There are large MSU/AMSU differences, with widely varying behavior for land and ocean averages. After the CCM3 diurnal adjustments are applied, the difference time series are more similar to each other for land and ocean averages, but large trends remain. Applying the DIUR_OPT adjustments reduces the trends slightly (Fig. 7c) and makes the land and ocean time series more similar, but the trend is still present. There are several possible explanations for these differences that we can exclude with simple analysis:

- Residual errors in the diurnal adjustment. The similarity of the differences for land and ocean scenes suggests that the cause is not related to problems with the diurnal adjustments.
- Errors in the *NOAA-14* target factor. The target factor is a calibration target-dependent adjustment we use to account for instrument nonlinearity. Because the target temperature for *NOAA-14* has a strong trend during 1999–2004, an error in the target factor could lead to a spurious trend in the *NOAA-14* radiances. Such an error would cause large oscillations in the MSU minus AMSU differences (see Fig. S5).
- Differing temperature trends in the atmosphere as a function of height. Temperature trends that vary with height coupled with the slightly different temperature weighting functions for MSU2 and AMSU5 might lead to difference trends between MSU and AMSU. A study of simulated radiances calculated from reanalysis output (see Fig. S6) shows that the observed differences are far too large to be explained by this effect.

We are left with explanation that the differences are caused by a calibration in either *NOAA-14* or *NOAA-15* (or both). Our baseline dataset will use both MSU and AMSU measurements during the overlap period. If we

exclude MSU data after 1999 (implicitly assuming the error is due to *NOAA-14*), the long-term trend decreases by 0.019 K decade^{-1}, and if we exclude AMSU data before 2003 (implicitly assuming the error is due to *NOAA-15*), the long-term trend increases by 0.01 K decade^{-1}).

5. Results

a. Results for MSU and AMSU separately

In Tables 2 and 3 we present a summary of near-global trends (80°S–80°N; 1999–2013) for different levels of adjustment. For AMSU, these results were already discussed in section 4b. For both MSU and AMSU, applying the DIUR_OPT adjustment has a similar effect of increasing the ocean trend slightly, and bringing the land trends computed using different modeled diurnal cycles closer together. Table 4 presents the near-global trends (80°S–80°N, 1979–2014) for the combined MSU/AMSU results for both the model adjusted and optimized versions. Again, the DIUR_OPT method tends to increase ocean trends slightly, and to bring then land trends computed from the different diurnal adjustments closer together.

For the previous version of our dataset (V3.3) we performed a detailed uncertainty analysis (Mears et al. 2011) that included contributions from the uncertainty from the satellite-specific bias and nonlinearity adjustments, sampling uncertainty, the relative drift during the MSU/AMSU overlap period, and uncertainty in the model-based diurnal adjustments. The 2-sigma uncertainty for the global mean trend in TMT from this work was ±0.042 K decade^{-1}. While we have not yet completed a similar analysis for the current method, we expect that the formal uncertainty in the global mean trend would be slightly reduced, since the part of the
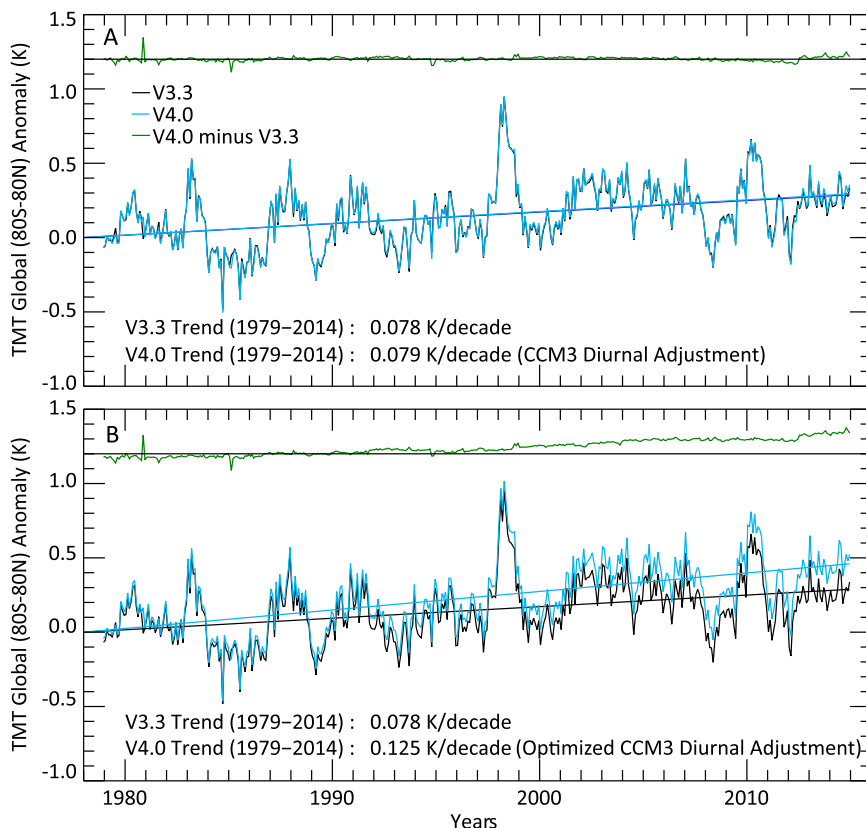
FIG. 8. Comparison between RSS V3.3 global (80°S–80°N) anomaly time series, and results from the V4.0 merging algorithm with different levels of adjustments applied.

uncertainty due to the diurnal adjustments is reduced by the optimization procedure.

b. Comparison with version 3.3

In Fig. 8, we show global time series comparisons of the V4.0 combined MSU/AMSU dataset with various levels of adjustment applied to the previous version, V3.3. Figure 8a shows the comparison when the unadjusted CCM3 diurnal climatology is used. This approach is a close parallel to V3.3 and small differences were expected. The time series are very similar, with a few months of differences more than 0.1 K, which likely result from slightly different data availability of the V4.0 dataset, which was obtained from the NOAA CLASS system compared to the V3.3 dataset, which was obtained informally from NOAA personnel. There is also a small relative trend from 2010 to mid-2012. This is due to the exclusion of the rapidly drifting post-2009 *Aqua* data from V4.0, and to the inclusion of data from *NOAA-19* and *MetOp-B* in V4.0. The agreement shown here supports the assertion made in section 3c that changes in the number of fields of view used in the analysis does not lead to important differences in long-term trends.

Figure 8b shows the comparison after the diurnal optimization has been applied to both MSU and AMSU. The overall trend increases from 0.079 to 0.125 K decade^{-1} is caused by an overall slope increase for both MSU and AMSU, and a small jump in 2012 when AMSU data from *MetOp-B* start to be included.

c. Comparison with other MSU/AMSU-derived datasets

In Fig. 9 we show a comparison between the results of this work (RSS V4.0), and datasets produced by other research groups. These are University of Alabama, Huntsville (UAH), version 5.6 (Christy et al. 2007; Christy et al. 2001), NOAA's Satellite Applications and Research (STAR), version 3.0 (Zou et al. 2009), and University of Washington (UW) version 1.0 (Po-Chedley et al. 2015). We show results for both near-global (80°S–80°N) averages and tropical averages (30°S–30°N). Note that the UW dataset is only available over the 30°S–30°N latitude range. Over both regions, RSS V4.0 is in good agreement with STAR 3.0 until about 2000, when the effects of the diurnal optimization become more important. This is not surprising, because the STAR method uses a slightly scaled version of the
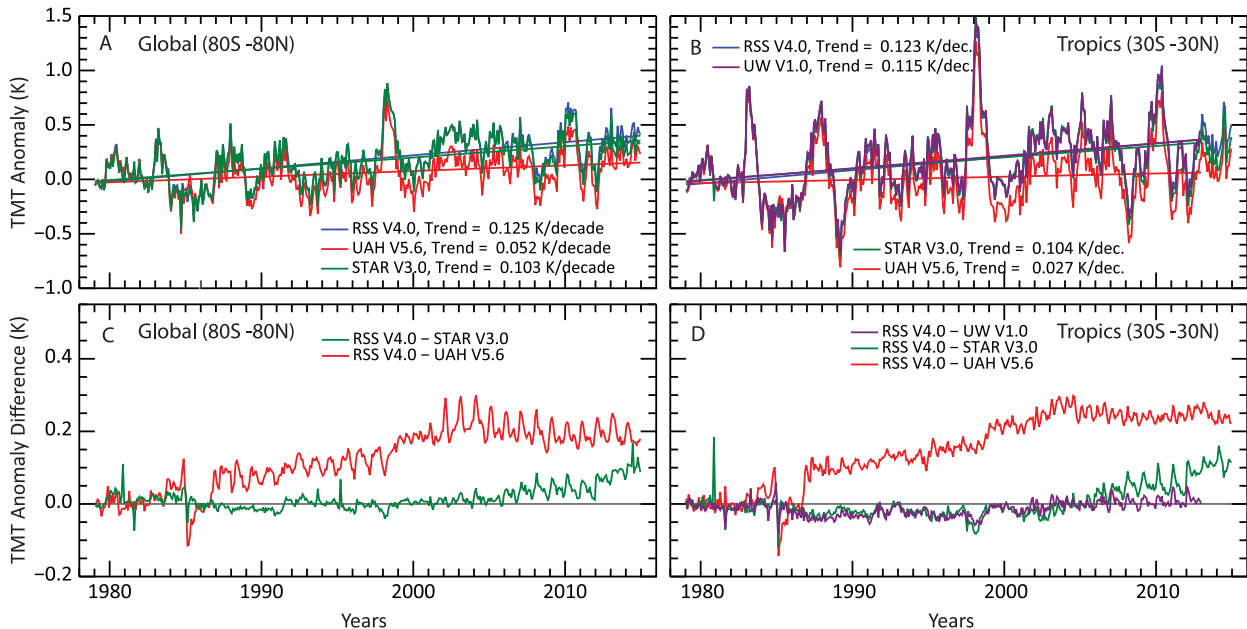
FIG. 9. Comparisons of near-global (80°S–80°N) and tropical (30°S–30°N) anomaly time series for TMT datasets produced by different groups. To make differences in trends easier to see, the anomaly time series have been adjusted so that their averages over 1979 are zero.

RSS diurnal climatology to perform diurnal adjustments, and thus is similar to RSS V3.3 during this period. There are much larger differences relative to the UAH data, particularly during 1985–87, and during the 1990s. The earlier difference is mostly due to large differences in the target factor adjustment for the *NOAA-09* satellite between our two groups (Po-Chedley and Fu 2012). The cause of the later difference is likely due to differences in the diurnal adjustments during the *NOAA-11* mission, which drifted over 6 h in measurement time over this period. After 2000, we speculate that the differences are due to a combination of different diurnal adjustment strategies and different choices about which instruments to include in the merged product. In the tropics, the UW dataset and the STAR dataset closely track each other until about 2004. This is not surprising, since the UW data use the STAR L1C calibrated radiances as input to their algorithm. After 2004, the two datasets diverges, as the diurnal adjustment procedure becomes more important. After 2004, RSS V4.0 is in much better agreement with the UW data than with either of the other two datasets. This is likely because both products use optimized diurnal adjustment based on the satellite observations.

d. Comparison with total column water vapor

Over the tropical oceans, atmospheric temperature and total column water vapor (TCWV) are tightly constrained assuming near-constant relative humidity and the Clausius–Clapeyron relationship (Mears et al. 2007;

Wentz and Schabel 2000). We can use this coupling to evaluate the consistency between satellite-observed total column water vapor and the various middle-troposphere temperature datasets. Mears et al. (2007) focused on the relationship between lower tropospheric temperature (TLT) and total column water vapor, and derived a climate model derived scaling ratio between the two variables. The focus of this paper is TMT, which has a weighting function that samples a thick layer of the atmosphere from the surface to the lower stratosphere so much of the information in TMT comes from a part of the atmosphere well above the bottom few kilometers of the tropical atmosphere where nearly all of the water vapor is located. Therefore, when we compare TMT to total column water vapor we are diagnosing both the Clausius–Clapeyron relationship between lower tropospheric temperature and TCWV, and the moist adiabatic lapse rate relationship (Santer et al. 2005) between lower tropospheric temperatures and the temperatures higher in the atmosphere that are measured by TMT.

For TCWV, we use the RSS version 7.0 retrievals of water vapor that are available from late 1987 onward. The vapor retrieval algorithm is described in Wentz and Spencer (1998) and Chelton and Wentz (2005) but uses an updated ocean surface model (Meissner and Wentz 2012). We construct monthly, ocean-only mean time series over the deep tropics (20°S–20°N), as well as TMT monthly time series over the same locations for each of the TMT datasets. These are shown in Fig. 10a. We

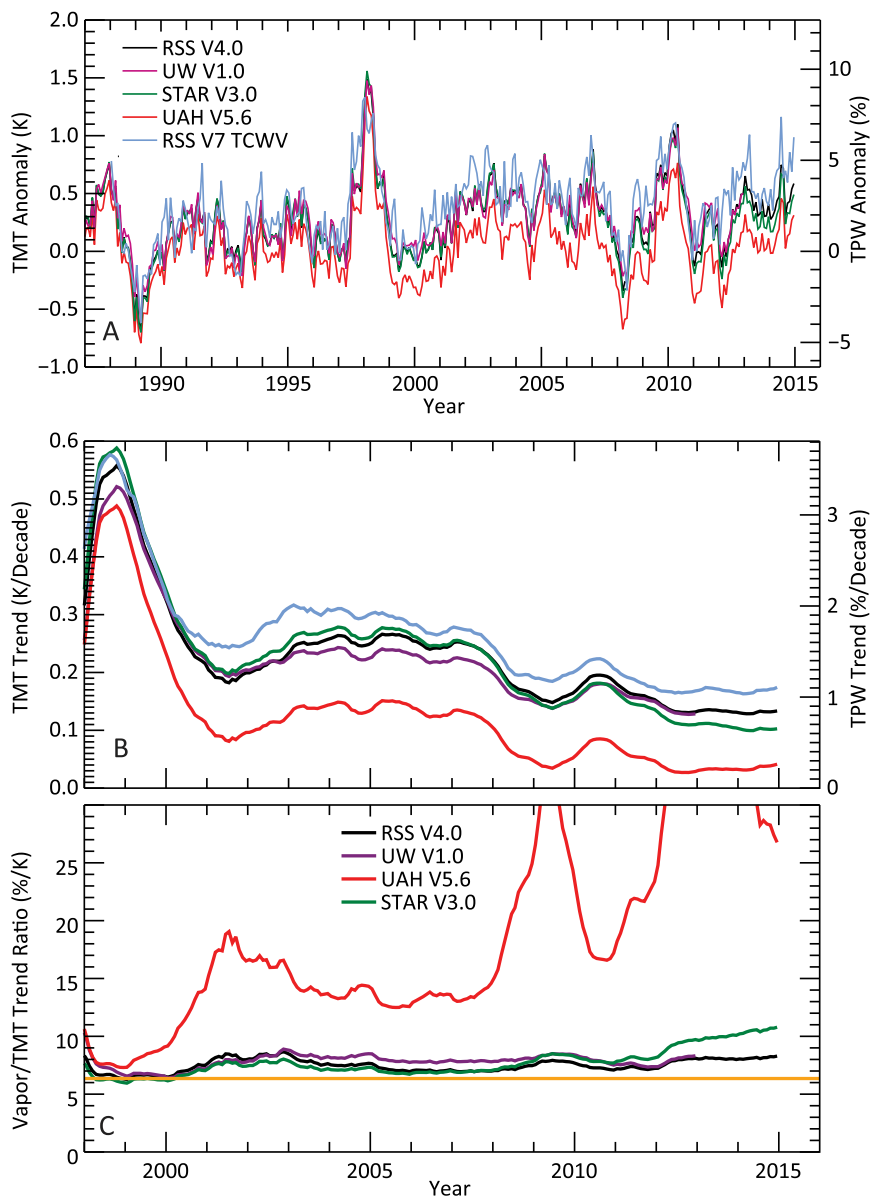FIG. 10. Comparison between TMT and TCWV over the oceans in the deep tropics (20°S–20°N). (a) TMT and TCWV anomaly time series over the 1988–2014 period. (b) Running linear trends with the trend starting point set to January 1988, and the trend ending point equal to the value on the *x* axis. (c) Ratio of TCWV to TMT running trends as a function of trend ending point. Note that this ratio tends to exaggerate discrepancies when the TMT trend approaches zero, as it does for the UAH dataset.

restrict our attention to the deep tropics because we are not confident that the near-surface and TMT temperatures are as tightly coupled in regions where the atmospheric dynamics are not dominated by convection.

We then evaluate the scaling ratio between TCWV and TMT on intermediate time scales. To do this, we filter the anomaly time series to remove variability on time scales both longer than 3 years and shorter than 3 months using a digital filter (Lynch and Huang

1992). We then estimate the scaling ratio between TCWV and TMT by computing the ratio of standard deviation for each time series as was done in Mears et al. (2007). When this is done for the RSS vapor paired with each of the TMT datasets, the results are tightly clustered between 6.0 and 6.6, indicating a consistent scaling behavior between the different TMT datasets and water vapor on short time scales (see Table S1).

To evaluate the scaling ratio on longer time scales we investigate running trends of TCWV and TMT. Figure 10b shows running trends of tropical (20°S–20°N) oceanic water vapor and TMT anomalies. Each point plotted on the graph is the trend, starting in January 1988 and ending at the time indicated on the *x* axis. The *y* axis for the vapor measurements is scaled so that a 1° change in temperature produces a 6.35% change in water vapor. From this figure it is easy to conclude that there is correlation between TCWV and TMT on short time scales by noting the correspondence between the fluctuations in each running mean. The datasets disagree on longer time scales. This is clear in Fig. 10c, which shows the ratio of the running vapor trends divided by the running TMT trends for each of the TMT datasets. If the scaling on longer time scales were the same as on intermediate time scales, then the ratio line would be close to the horizontal orange line at $6.35\% \, K^{-1}$. The RSS V4.0 and UW V1.0 curves lie slightly above this value. The STAR V3.0 is higher, with the value approaching 10.0 by 2015. The UAH curve is much higher, indicating that the long-term trends in the UAH dataset are too low to be consistent with the measured water vapor of the period since 1988.

6. Discussion and conclusions

We have shown that the long-term changes in MSU/AMSU-derived atmospheric temperatures depend strongly on the details of the adjustments applied to account for changing measurement time. We showed that diurnal adjustments based on general circulation model output are not sufficiently accurate to remove the effects of measurement time drift. This investigation also revealed that two satellites, *NOAA-15* and *Aqua*, likely suffered from calibration drifts late in their respective missions. We compared three different approaches to account for the shortcomings of the model-based diurnal adjustments. All three approaches lead to similar results for the AMSU measurements, increasing our confidence in our chosen method, which optimizes the model-derived diurnal cycles by computing a second harmonic adjustment. Using this method, we have introduced a new version of the RSS TMT dataset. The resulting dataset shows more warming than the previous version of the dataset, particularly after 1998. We also eliminated the use of *NOAA-15* data after December 2011 and *Aqua* data after December 2009. The combined effect of this data editing is to reduce the amount of warming in the final merged product. Our method shows similar final results when different diurnal cycle climatologies are used as the starting point, suggesting that the method converges toward a common optimal

result. In the tropics, the new dataset agrees well with the UW dataset, which was constructed using different methods but with a similar goal of deducing the needed diurnal adjustments from the satellite measurements themselves. Both the UW and RSS datasets agree more closely with estimates of changes in total column water vapor than the STAR and UAH datasets.

7. Data availability

The RSS V4.0 TMT dataset, along with an image browser and time series viewers, is available online (http://www.remss.com/measurements/upper-air-temperature).

REFERENCES

Chelton, D. B., and F. J. Wentz, 2005: Global microwave satellite observations of sea surface temperature for numerical weather prediction and climate research. *Bull. Amer. Meteor. Soc.*, **86**, 1097–1115, doi:10.1175/BAMS-86-8-1097.

Christy, J. R., R. W. Spencer, and W. D. Braswell, 2000: MSU tropospheric temperatures: Dataset construction and radiosonde comparisons. *J. Atmos. Oceanic Technol.*, **17**, 1153–1170, doi:10.1175/1520-0426(2000)017<1153:MTTDCA>2.0.CO;2.

——, D. E. Parker, S. J. Brown, I. Macadam, M. Stendel, and W. B. Norris, 2001: Differential trends in tropical sea surface and atmospheric temperatures since 1979. *Geophys. Res. Lett.*, **28**, 183–186, doi:10.1029/2000GL011167.

——, R. W. Spencer, W. B. Norris, W. D. Braswell, and D. E. Parker, 2003: Error estimates of version 5.0 of MSU–AMSU bulk atmospheric temperatures. *J. Atmos. Oceanic Technol.*, **20**, 613–629, doi:10.1175/1520-0426(2003)20<613:EEOVOM>2.0.CO;2.

——, W. B. Norris, R. W. Spencer, and J. J. Hnilo, 2007: Tropospheric temperature change since 1979 from tropical radiosonde and satellite measurements. *J. Geophys. Res.*, **112**, D06102, doi:10.1029/2005JD006881.

Johns, T. C., and Coauthors, 2006: The New Hadley Centre Climate Model (HadGEM1): Evaluation of coupled simulations. *J. Climate*, **19**, 1327–1353, doi:10.1175/JCLI3712.1.

Kiehl, J. T., J. J. Hack, G. B. Bonan, B. A. Boville, B. P. Briegleb, D. L. Williamson, and P. J. Rasch, 1996: Description of the NCAR Community Climate Model (CCM3). NCAR Tech. Note NCAR/TN-420+STR, 152 pp., doi:10.5065/D6FF3Q99.

Kottayil, A., V. O. John, and S. A. Buehler, 2013: Correcting diurnal cycle aliasing in satellite microwave humidity sounder measurements. *J. Geophys. Res. Atmos.*, **118**, 101–113, doi:10.1029/2012JD018545.

Lindfors, A. V., I. A. Mackenzie, S. F. B. Tett, and L. Shi, 2011: Climatological diurnal cycles in clear-sky brightness temperatures from the High-Resolution Infrared Radiation Sounder (HIRS). *J. Atmos. Oceanic Technol.*, **28**, 1199–1205, doi:10.1175/JTECH-D-11-00093.1.

Lynch, P., and X. Y. Huang, 1992: Initialization of the HIRLAM model using a digital filter. *Mon. Wea. Rev.*, **120**, 1019–1034, doi:10.1175/1520-0493(1992)120<1019:IOTHMU>2.0.CO;2.

Martin, G. M., M. A. Ringer, V. D. Pope, A. Jones, C. Dearden, and T. J. Hinton, 2006: The physical properties of the atmosphere in the new Hadley Centre Global Environmental Model, HadGEM1. Part 1: Model description and global climatology. *J. Climate*, **19**, 1274–1301, doi:10.1175/JCLI3636.1.

Mears, C. A., and F. J. Wentz, 2005: The effect of diurnal correction on satellite-derived lower tropospheric temperature. *Science*, **309**, 1548–1551, doi:10.1126/science.1114772.

——, and ——, 2009: Construction of the Remote Sensing Systems V3.2 atmospheric temperature records from the MSU and AMSU microwave sounders. *J. Atmos. Oceanic Technol.*, **26**, 1040–1056, doi:10.1175/2008JTECHA1176.1.

——, B. D. Santer, F. J. Wentz, K. E. Taylor, and M. F. Wehner, 2007: Relationship between temperature and precipitable water changes over tropical oceans. *Geophys. Res. Lett.*, **34**, L24709, doi:10.1029/2007GL031936.

——, F. J. Wentz, P. Thorne, and D. Bernie, 2011: Assessing uncertainty in estimates of atmospheric temperature changes from MSU and AMSU using a Monte-Carlo estimation technique. *J. Geophys. Res.*, **116**, D08112, doi:10.1029/2010JD014954.

Meissner, T., and F. J. Wentz, 2012: The emissivity of the ocean surface between 6 and 90 GHz over a large range of wind speeds and Earth incidence angles. *IEEE Trans. Geosci. Remote Sens.*, **50**, 3004–3026, doi:10.1109/TGRS.2011.2179662.

Po-Chedley, S., and Q. Fu, 2012: A bias in the midtropospheric channel warm target factor on the NOAA-9 microwave sounding unit. *J. Atmos. Oceanic Technol.*, **29**, 646–652, doi:10.1175/JTECH-D-11-00147.1.

——, T. J. Thorsen, and Q. Fu, 2015: Removing diurnal cycle contamination in satellite-derived tropospheric temperatures: Understanding tropical tropospheric trend discrepancies. *J. Climate*, **28**, 2274–2290, doi:10.1175/JCLI-D-13-00767.1.

Rienecker, M. M., and Coauthors, 2011: MERRA: NASA's Modern-Era Retrospective Analysis for Research and Applications. *J. Climate*, **24**, 3624–3648, doi:10.1175/JCLI-D-11-00015.1.

Santer, B. D., and Coauthors, 2005: Amplification of surface temperature trends and variability in the tropical atmosphere. *Science*, **309**, 1551–1556, doi:10.1126/science.1114867.

Wentz, F. J., and M. C. Schabel, 1998: Effects of orbital decay on satellite-derived lower-tropospheric temperature trends. *Nature*, **394**, 661–664, doi:10.1038/29267.

——, and R. W. Spencer, 1998: SSM/I rain retrievals within a unified all-weather ocean algorithm. *J. Atmos. Sci.*, **55**, 1613–1627, doi:10.1175/1520-0469(1998)055<1613:SIRRWA>2.0.CO;2.

——, and M. C. Schabel, 2000: Precise climate monitoring using complementary satellite data sets. *Nature*, **403**, 414–416, doi:10.1038/35000184.

Zou, C.-Z., and W. Wang, 2011: Intersatellite calibration of AMSU-A observations for weather and climate applications. *J. Geophys. Res.*, **116**, D23113, doi:10.1029/2011JD016205.

——, M. Gao, and M. D. Goldberg, 2009: Error structure and atmospheric temperature trends in observations from the Microwave Sounding Unit. *J. Climate*, **22**, 1661–1681, doi:10.1175/2008JCLI2233.1.